

Phonon dispersions and Fermi surfaces nesting explaining the variety of charge ordering in titanium-oxypnictides superconductors

Kousuke Nakano¹, Kenta Hongo¹, and Ryo Maezono¹

¹ School of Information Science, JAIST, Asahidai 1-1, Nomi, Ishikawa 923-1292, Japan. Correspondence and requests for materials should be addressed to K.N. (email:kousuke_1123@icloud.com) or R.M. (email:rmaezono@mac.com)

(Dated: March 4, 2024)

There has been a puzzle between experiments and theoretical predictions on the charge ordering of layered titanium-oxypnictides superconductors. Unconventional mechanisms to explain this discrepancy have been argued so far, even affecting the understanding of superconductivity on the compound. We provide a new theoretical prediction, by which the discrepancy itself is resolved without any complicated unconventional explanation. Phonon dispersions and changes of nesting vectors in Fermi surfaces are clarified to lead to the variety of superlattice structures even for the common crystal structures when without CDW, including orthorhombic $2 \times 2 \times 1$ one for $\text{BaTi}_2\text{As}_2\text{O}$, which has not yet been explained successfully so far, being different from tetragonal $\sqrt{2} \times \sqrt{2} \times 1$ for $\text{BaTi}_2\text{Sb}_2\text{O}$ and $\text{BaTi}_2\text{Bi}_2\text{O}$. The electronic structure analysis can naturally explain experimental observations about CDW including most latest ones without any cramped unconventional mechanisms.

Layered titanium oxypnictides, $\text{ATi}_2\text{Pn}_2\text{O}$ [$A = \text{Na}_2, \text{Ba}, (\text{SrF})_2, (\text{SmO})_2$; $\text{Pn} = \text{As}, \text{Sb}, \text{Bi}$], [1–7] have the common undistorted structure, as shown in Fig. 1, including Ti_2O -plane that leads to quasi two-dimensional (2D) electronic structures. Yajima *et al.* [5] synthesized $\text{BaTi}_2\text{Sb}_2\text{O}$ and reported its superconductivity with the transition temperature, $T_c = 1.2$ K. Doan *et al.* [6] also synthesized $\text{Ba}_{(1-x)}\text{Na}_x\text{Ti}_2\text{Sb}_2\text{O}$ individually and reported its superconductivity with $T_c = 5.5$ K. Followed by their pioneering works, similar kinds of compounds, $\text{BaTi}_2\text{Bi}_2\text{O}$, $\text{BaTi}_2(\text{Sb}_{1-x}\text{Bi}_x)_2\text{O}$, $\text{BaTi}_2(\text{Sb}_{1-x}\text{Sn}_x)_2\text{O}$, $\text{Ba}_{1-x}\text{K}_x\text{Ti}_2\text{Sb}_2\text{O}$, and $\text{Ba}_{1-x}\text{Rb}_x\text{Ti}_2\text{Sb}_2\text{O}$, have been synthesized to get superconductivities, achieving the current highest T_c around 6.1 K. [7–12] Based on Allen-Dynes formalism [13, 14] within DFT, Subedi suggested a conventional BCS-type superconductivity mechanism holds in $\text{BaTi}_2\text{Sb}_2\text{O}$. [15] This theoretical finding was supported afterward by experiments of specific heats, NMR, and μSR [16–18], confirming full-gap BCS mechanism with s -wave pairing for this compound. Although their T_c values themselves are relatively low compared with possibly conventional BCS-type mechanism, the superconductivity of $\text{BaTi}_2\text{Sb}_2\text{O}$ and its relatives attracts special interests in the sense that their nominal electronic configurations, $\text{Ti}^{3+}(d^1)$, are conjugate with those for cuprates superconductors [19] with respect to the electron-hole symmetry. Quasi 2-dimensional (2D) transports in these systems also attract the common interest among those for cuprates [19] as well as for iron arsenides superconductors [20], leading to the arguments on the similarity of superconducting mechanisms. [5, 6]

The possibilities of the density waves (DW) in these systems are one of the key concepts, which is common to low-dimensional transports possible for cuprates and iron arsenides. Anomalies in the temperature dependence of resistivity $\rho(T)$ and magnetic susceptibility $\chi(T)$ at low temperature are sometimes observed in these systems, getting into an argument over if the anomalies can be attributed to the emergence of charge density waves (CDW) or spin density

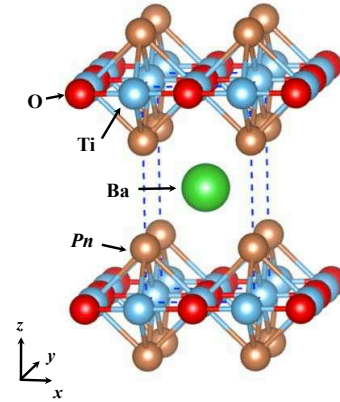


FIG. 1. Undistorted crystal structures of $\text{BaTi}_2\text{Pn}_2\text{O}$ ($\text{Pn} = \text{As}, \text{Sb}, \text{and Bi}$). Crystal symmetry is $P4/mmm$ (No.123).

waves (SDW). [1, 2, 4–6] Several DFT studies applied to $\text{BaTi}_2\text{As}_2\text{O}$ and $\text{BaTi}_2\text{Sb}_2\text{O}$ [21–23] have reported the possibility of SDW, while it has not yet been observed experimentally, such as by NMR/NQR for $\text{Sb}^{121/123}$ and μSR for $\text{BaTi}_2\text{As}_2\text{O}$ and $\text{BaTi}_2\text{Sb}_2\text{O}$. [16–18] Focusing on CDW, the nesting of Fermi surface matters, which is enhanced by 2D nature of Ti_2O planes. While conventional models take a simple picture of 2D transport with $\text{Ti}-3d_{xy}$ orbital only, [5] Singh [21] clarified a more complicated 3D shape of Fermi surface in $\text{BaTi}_2\text{Sb}_2\text{O}$ by taking into account several $\text{Ti}-3d$ orbitals contributions. A similar shape was also predicted in $\text{BaTi}_2\text{Bi}_2\text{O}$, theoretically [24]. Indeed, such shapes have been recently observed by state-of-the-art Angle-Resolved Photo Emission Spectroscopy (ARPES) applied to $\text{BaTi}_2\text{As}_2\text{O}$ and $\text{BaTi}_2\text{Sb}_2\text{O}$ single crystals. [25, 26] Subedi [15] worked on $\text{BaTi}_2\text{Sb}_2\text{O}$ using DFT and reported the possible lattice instability toward CDW with $\sqrt{2} \times \sqrt{2} \times 1$ superstructure at low temperature. Experimentally, however, no such superlattice peaks were found by neutron and electron diffractions for this compound, [17, 27] reviving the argument over if the anoma-

lies in $\rho(T)$ and $\chi(T)$ can be really attributed to the phonon-driven CDW or not. Though Frandsen *et al.* [27] observed tiny lattice displacements from tetragonal to orthorhombic in both $\text{BaTi}_2\text{As}_2\text{O}$ and $\text{BaTi}_2\text{Sb}_2\text{O}$, theoretically predicted $\sqrt{2} \times \sqrt{2} \times 1$ superlattice peaks [15] could not be found experimentally. To account for this, they proposed a bit complicated picture that the intra-unit-cell nematic charge order, such as that observed in cuprates [28, 29], might be the origin of the anomalies in $\rho(T)$ and $\chi(T)$.

Another important topic on this system is the 'two-dome' structure in the dependence of $T_c(x)$ on the concentration of ionic substitutions, $Pn = \text{Sb}_x\text{Bi}_{(1-x)}$ in $\text{BaTi}_2Pn_2\text{O}$. [8] Similar 'two-dome' structures are known also for cuprates [30–34] and iron arsenides [35, 36] superconductors. The 'two-dome' structure can be regarded as a modification with a singularity put on the original single peak dependence. The singularity might be attributed to electron or spin orderings such as DW transition. Actually, a series of NMR experiments on $\text{LaFeAsO}_{1-x}\text{H}_x$ [37] identified the peak as being corresponding to the emergence of the new SDW phase related to the second T_c dome. This suggests that another origin of the second dome be different from that of the first dome. The 'two-dome' for $\text{BaTi}_2Pn_2\text{O}$, on the other hand, has not well been investigated so far.

As mentioned above, the layered titanium oxypnictides superconductors show a lot of similar phenomena to cuprates and iron-arsenides superconductors. The investigation of DW transition in these oxypnictides could then be one of the most important clues to understanding of the physics of high- T_c superconducting mechanism. In the present study, we investigated the possibility of DW transition in $\text{BaTi}_2Pn_2\text{O}$ ($Pn = \text{As, Sb, Bi}$) using DFT-based phonon analysis. Because of the common lattice structure when without DW, we could perform systematic and careful comparisons among the three compounds, putting the same computational conditions to suppress artifacts as less as possible. As a result, we found a new possibility of orthorhombic $2 \times 2 \times 1$ superlattice structure for $\text{BaTi}_2\text{As}_2\text{O}$, which is different from the previous prediction by Subedi [15] for $\text{BaTi}_2\text{Sb}_2\text{O}$, tetragonal $\sqrt{2} \times \sqrt{2} \times 1$. Our theoretical finding can provide a more natural explanation for the structural transition and the weak superlattice peaks observed by Frandsen *et al.* [27] in terms of the conventional phonon-driven CDW, not by such a complicated mechanism as intra-unit-cell nematic charge ordering, as given in their papers. [28, 29] The finding might also account for the anomalies of $\rho(T)$ and $\chi(T)$ being attributed to the lattice instability. While $\text{BaTi}_2\text{Bi}_2\text{O}$ does not show anomalies in $\rho(T)$ and $\chi(T)$, we found lattice instability possibly inducing tetragonal $\sqrt{2} \times \sqrt{2} \times 1$ superlattice structure. Such a discrepancy is observed in a $\text{LaO}_{0.5}\text{F}_{0.5}\text{BiS}_2$ superconductor as well. [45] To account for this, Yildirim [38] argued the possibility of an unconventional superconducting mechanism in which the inherent lattice instability plays an important role in the Cooper pairing. The similarity of the discrepancy for the present case might imply the similar unconventional mechanism for

$\text{BaTi}_2\text{Bi}_2\text{O}$.

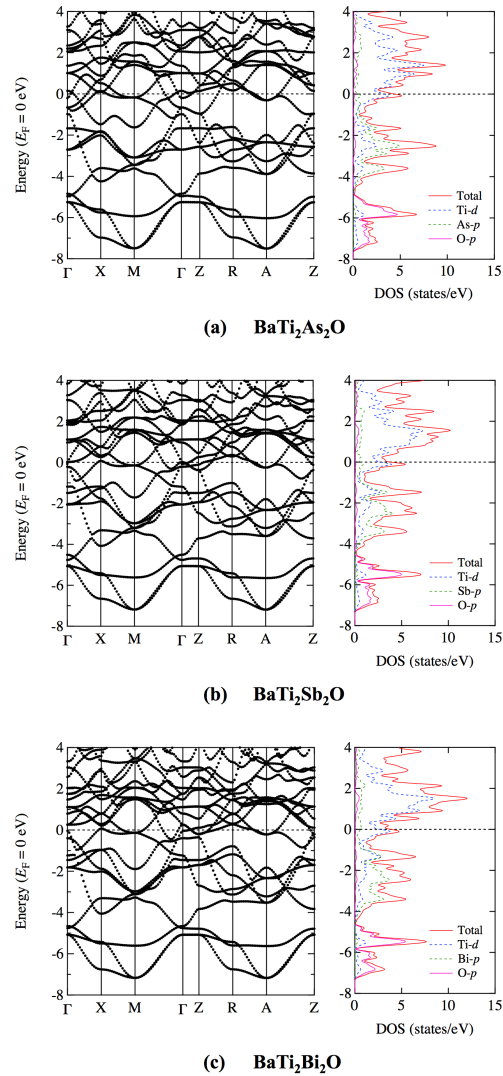


FIG. 2. Electronic band structures and densities of states for $\text{BaTi}_2Pn_2\text{O}$ ($Pn =$ (a) As, (b) Sb, and (c) Bi) under $P4/mmm$ symmetry. Each Fermi energy is defined as zero.

RESULTS

Lattice instabilities from undistorted structures

Electronic band structures and densities of states (DOS) for undistorted structures are shown in Fig. 2. Figure 3 highlights the corresponding Fermi surfaces with possible nesting vectors. Overall features agree well with previous DFT results by Yu *et al.* [23], Singh [21] and Suetin *et al.* [24] for each compound, justifying no specific artifacts due to any choices of computational conditions. Note that our optimized geometry parameters are also in good agreements with the previous calculations (See Supplementary Note 1).

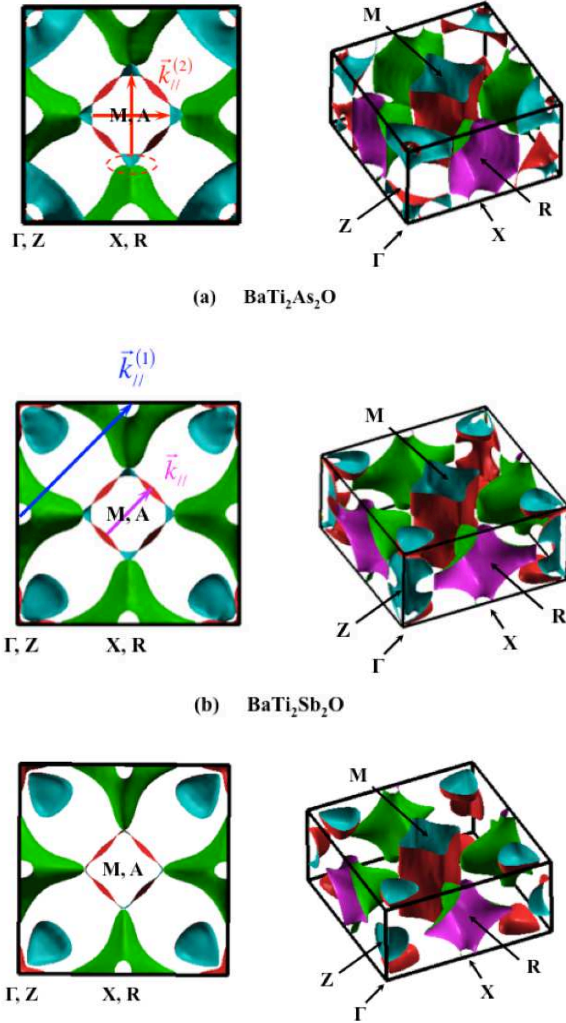


FIG. 3. Fermi surfaces of $\text{BaTi}_2Pn_2\text{O}$ under $P4/mmm$ symmetry ($Pn =$ (a) As, (b) Sb, and (c) Bi). Possible nesting vectors are also depicted (see text for notation). Note that Γ point is located at the corner, as shown in the figure.

Phonon dispersions for undistorted structures are shown in Fig. 4. Despite the common crystal structure, we see that the phonon instabilities appear around different points, M and A for $Pn =$ Sb, Bi, while X and R for $Pn =$ As [hereafter, all the \vec{k} and \vec{q} points are labeled according to Brillouin-zone database on the *Bilbao Crystallographic Server* [46]]. The former instabilities (for $Pn =$ Sb, Bi) are consistent with the previous calculations by Subedi [15] on $Pn =$ Sb. The latter instability (for $Pn =$ As), on the other hand, has been never reported before, so we carefully examined to confirm that the result does not depend on the choice of pseudo potentials. For $Pn =$ Sb and Bi, the instability occurs around M and A , corresponding to $(q_x, q_y) = (1/2, 1/2)$ [hereafter a unit of \vec{q} is $2\pi/a$]. For q_z direction, there is no specific dependence, as shown in the dispersion along M to A in the right panel of Fig. 4 (b) and (c). From phonon pDOS (par-

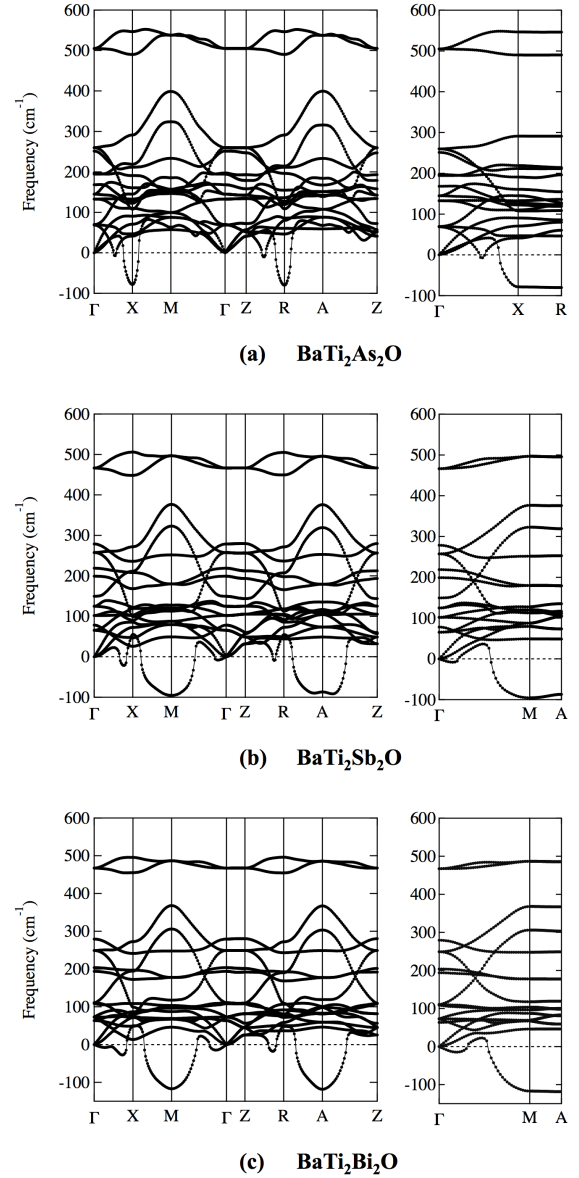


FIG. 4. Phonon dispersions of $\text{BaTi}_2Pn_2\text{O}$ under $P4/mmm$ symmetry ($Pn =$ (a) As, (b) Sb, and (c) Bi).

tical DOS), we can identify which vibration modes lead to the instability toward the superlattice. It is found from phonon pDOS that the negative (imaginary) frequencies mainly come from Ti 'in-plane' (within xy plane) vibrations (See Supplementary Note 2). We therefore concentrate on the representative case with M , $(q_x, q_y, q_z) = (1/2, 1/2, 0)$, corresponding to $\sqrt{2} \times \sqrt{2} \times 1$ superlattice structure. By analyzing the dynamical matrices, we can further identify the superlattice structure shown in Fig. 5. Note that this is the same structure as that predicted previously by Subedi [15] for $Pn =$ Sb.

The same scheme is applied to $Pn =$ As with the instability around X and R , corresponding to $(q_x, q_y) = (0, 1/2)$: For q_z direction, there is no specific dependence, as shown in

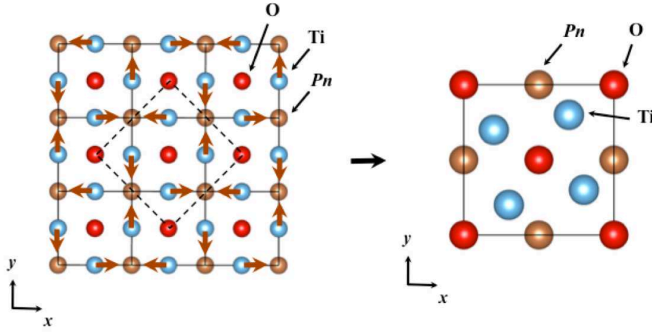


FIG. 5. Atomic displacements corresponding to the negative (imaginary) phonon mode at M ($1/2, 1/2, 0$) point, leading to $\sqrt{2} \times \sqrt{2} \times 1$ superlattice for $\text{BaTi}_2\text{Pn}_2\text{O}$ ($Pn = \text{Sb}$ and Bi). Dashed lines in the left panel stand for the unit cell of the superlattice, drawn in the right panel again with displaced atomic positions after the rotation by 45 degree. Symmetry of the superlattice is $P4/mbm$ (No.127).

the dispersion along X to R in the right panel of Fig. 4 (a). From phonon pDOS, we can identify that the vibrations for the instability come from Ti and As 'in-plane' vibrations (See Supplementary Note 2). We therefore take a representative mode at X , $(q_x, q_y, q_z) = (0, 1/2, 0)$. By analyzing the dynamical matrices, we get the superlattice structure shown in Fig. 6, $1 \times 2 \times 1$ superlattice.

Superlattice structures and T_c

The negative modes appearing in Fig. 4 are expected to disappear when we further relax the lattices along the negative modes to get superlattices. Resultant phonon dispersions are shown in Fig. 7. For $\sqrt{2} \times \sqrt{2} \times 1$ superlattices of Bi and Sb, the negative modes have disappeared assuring the superlattice as the final stable structures [the negative mode seen around Γ for Bi is due to the well-known artifact coming from the discreteness of Fast Fourier Transform (FFT) grid]. For As, on the other hand, the negative modes at X and U point still remain. Taking the representative X point, this implies the further superlattice transition toward $2 \times 2 \times 1$. The phonon pDOS analysis shows that the superlattice deformation still comes from 'in-plane' vibrations of Ti and As, actually leading to the superlattice structure as shown in Fig. 8. The geometry optimization along this deformation gives lattice parameters, $a = 8.122 \text{ \AA}$, $b = 8.108 \text{ \AA}$, and $c = 7.401 \text{ \AA}$ (See Supplementary Note 4). The orthorhombicity parameter is $\eta = 2 \times (a - b)/(a + b) = 0.171\%$. To finalize the verification, we ought to examine if the negative modes surely disappear in the $2 \times 2 \times 1$ superlattice. It was, however, intractable because four times enlarged unit cell requires 4^3 times more computational cost and lower symmetry makes more demands for k - and q -mesh samplings over larger reciprocal space.

Superconducting transition temperatures, T_c , are estimated using Allen-Dynes formula [14], as shown in Table VI in Sup-

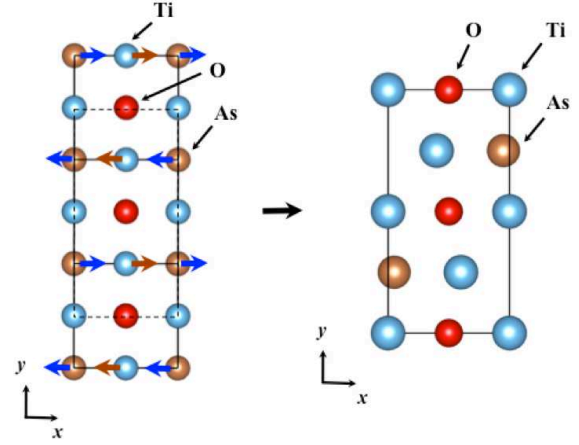


FIG. 6. Atomic displacements corresponding to the negative (imaginary) phonon mode at X ($0, 1/2, 0$) point, leading to $1 \times 2 \times 1$ superlattice for $\text{BaTi}_2\text{As}_2\text{O}$. Dashed lines in the left panel stand for the unit cell of the superlattice, drawn in the right panel again with displaced atomic positions. Symmetry of the superlattice is $Pbmm$ (No.51).

plementary Information. The parameters used in the formula are also tabulated. Even with imaginary frequencies, T_c can be estimated just by ignoring the contributions [15], being the case for $1 \times 1 \times 1$. For $\sqrt{2} \times \sqrt{2} \times 1$ where all the negative modes disappear, the estimation gets to be more plausible. There seems, however, little change in the estimation from that in $1 \times 1 \times 1$. The present estimations, $T_c = 2.30$ (2.45) K for $Pn = \text{Sb}$ (Bi), are consistent with experiments reporting $T_c = 1.2$ (4.6) K for $Pn = \text{Sb}$ (Bi) [5, 7], as well as that by previous DFT study, $T_c = 2.7$ K for $Pn = \text{Sb}$ [15]. For $1 \times 2 \times 1$ ($Pn = \text{As}$), the estimation was made still under the existence of negative modes, and the more plausible estimation for $2 \times 2 \times 1$ was intractable as mentioned above. The estimations, $T_c = 6.93$ K ($1 \times 1 \times 1$) and 8.31 K ($1 \times 2 \times 1$) seem incompatible with experiments of $\text{BaTi}_2\text{As}_2\text{O}$ exhibiting no superconductivity so far. [4, 8] We might expect much lower T_c obtained for the $2 \times 2 \times 1$ superlattice structure.

DISCUSSIONS

Comparison with experiments

The orthorhombic $2 \times 2 \times 1$ superlattice structure, obtained here for $\text{BaTi}_2\text{As}_2\text{O}$, would attract interests in connection with experimental observations. Frandsen *et al.* actually observed a lattice structural transition from tetragonal $P4/mmm$ to orthorhombic $Pmmm$ by neutron diffractions. They also reported very weak superlattice peaks corresponding to $q_{Hx} = (1/2, 0, 0)$ or $q_{Hy} = (0, 1/2, 0)$ which disappears at higher temperatures by electron diffractions. [27] Since $\text{BaTi}_2\text{As}_2\text{O}$ has the same $P4/mmm$ parent structure as $\text{BaTi}_2\text{Sb}_2\text{O}$, they might expect a tetragonal $\sqrt{2} \times \sqrt{2} \times 1$ superlattice according to the

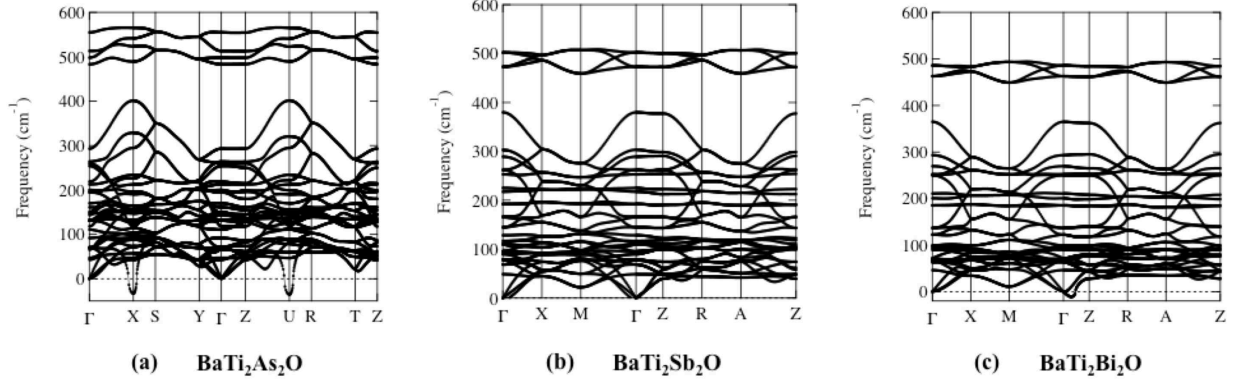


FIG. 7. Phonon dispersions of superlattice structure for $\text{BaTi}_2Pn_2\text{O}$ ($Pn =$ (a) As- $1 \times 2 \times 1$, (b) Sb- $\sqrt{2} \times \sqrt{2} \times 1$, and (c) Bi- $\sqrt{2} \times \sqrt{2} \times 1$).

previous DFT prediction by Subedi [15] for $Pn = \text{Sb}$. The lack of the expected $\sqrt{2} \times \sqrt{2} \times 1$ superlattice and the observation of the structural transition were explained by rather complicated mechanism such as intra-unit-cell nematic charge ordering, as an analogue of that in cuprates. [28, 29] The observed weak peaks of q_{H_x} or q_{H_y} was then regarded as being non-intrinsic, attributed to poly-crystalline grain boundary effects. Our finding of orthorhombic $2 \times 2 \times 1$ superlattice here can instead account for the observations, as intrinsic, more naturally in terms of the lattice instability due to conventional phonon-driven CDW. Note that our optimized geometry gives the orthorhombicity parameter, $\eta = 2 \times (a - b)/(a + b) = 0.171\%$, which is comparable with the experimental value $\eta = 0.22\%$ [27]. Though q_{H_x} or q_{H_y} is naturally explained, the present result also leads to the emergence of $q_{H_{xy}} = (1/2, 1/2, 0)$, which is not explicitly reported in the work by Frandsen *et al.* [27] Looking at their TEM photo in the paper, [27] it is actually quite difficult to distinguish the $q_{H_{xy}}$ peak from much brighter spots in the immediate vicinity. Polycrystalline sample qualities and weak intensities of the peak might also matter. We expect that further careful investigation would find $q_{H_{xy}}$ peak corresponding to the present $2 \times 2 \times 1$ superlattice structure.

Unlike $Pn = \text{As}$, the other two compounds are predicted to have $\sqrt{2} \times \sqrt{2} \times 1$ superlattices in our calculations, which is consistent with the preceding work by Subedi [15] for $Pn = \text{Sb}$. Then a question arises asking why only $Pn = \text{As}$ takes the different superlattice structure. This can be explained by the nesting of Fermi surfaces, shown in Fig. 3. Because of the cylindrical shape, every compound has a nesting vector $\vec{k}_{ij} = (k_x, k_y) = (1/4, 1/4)$ [hereafter a unit of \vec{k} is $2\pi/a$]. around M and A points, as previously pointed out by Yu *et al.* [23] for $Pn = \text{As}$. Another possible nesting around X and R is described by the vector $\vec{k}_{ij}^{(1)} = (1/2, 1/2)$, corresponding to the negative phonons we get around M and A in phonon Brillouin zones for $Pn = \text{Sb}$, Bi. This nesting has already been pointed out by Singh [21] and Subedi [15] for $Pn = \text{Sb}$. Looking carefully at the Fermi surface of $Pn = \text{As}$, we see the flattening of the cusp around X and R points (as shown by a dashed oval

in Fig.3 (a)), leading to new nesting vectors, $\vec{k}_{ij}^{(2)} = (0, 1/2)$ and $(1/2, 0)$. They correspond to the negative phonons around X and R appearing only for $Pn = \text{As}$. We note that $\vec{k}_{ij}^{(2)}$ have already been mentioned by Yu *et al.* [23] for $Pn = \text{As}$, but its relation to the phonon instability has not been discussed so far. Possible reasons why the flattening occurs only for As are discussed in the next section. Since all the above stories can be made only within the electronic Fermi surfaces, one might consider the phonon evaluations not necessarily required. We note, however, that there are several 2D chalcogenide systems where CDW cannot be explained only by the electronic Fermi surfaces, but accounted for when the phonon dispersions are evaluated. [39–43] We discuss this in the later section. It is further interesting if CDW superlattice transitions predicted here could be related to the anomalies of $\rho(T)$ and $\chi(T)$ at low temperature.

The $\sqrt{2} \times \sqrt{2} \times 1$ superlattice structure for $\text{BaTi}_2\text{Sb}_2\text{O}$ is predicted not only by the present work but also by Subedi [15]. However, such a superlattice has not yet been observed experimentally so far by any diffraction experiments such as neutron and electron diffractions. [17, 27] Frandsen *et al.* observed a subtle structural distortion from $P4/mmm$ to $Pmmm$ by neutron diffraction measurement at low temperature, [27] which is not consistent with the prediction. Note that all the above diffraction experiments are applied to polycrystalline samples. Interestingly, Song *et al.* has very recently reported the existence of $(1/2, 1/2)$ nesting vector by ARPES and STM measurements applied to high-quality single crystals, being consistent with the theoretical predictions. [26] The superlattice structure is hence expected to be detected by further diffraction measurements. The theoretically estimated distortion here is quite small, 0.14 \AA (See Supplementary Note 4), being in agreement with the previous calculation by Subedi, [15] so careful detections would be required for experiments. As described in the previous section, the estimated T_c is almost consistent with experiments, supporting that the compound is a conventional BCS-type superconductor, being consistent with the previous conclusion by Subedi. [15]

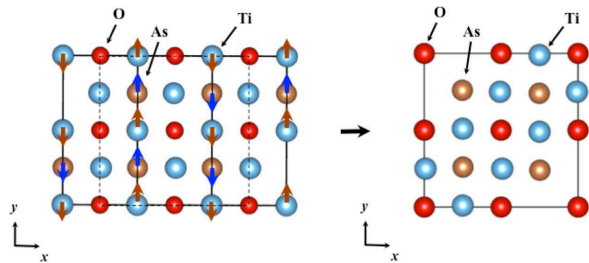


FIG. 8. Atomic displacements for $1 \times 2 \times 1$ $\text{BaTi}_2\text{As}_2\text{O}$ corresponding to the negative (imaginary) phonon mode at $X(1/2, 0, 0)$ point, leading to orthorhombic $2 \times 2 \times 1$ superlattice. Dashed lines in the left panel stand for the unit cell of the superlattice, drawn in the right panel again with displaced atomic positions. Symmetry of the $2 \times 2 \times 1$ superlattice is $Pbam$ (No.55).

In contrast to the other two compounds, there are little experiments on $\text{BaTi}_2\text{Bi}_2\text{O}$ because of the difficulty of sample preparation mainly due to the significant instability under the air and moisture. [7] As far as we have known, there is no previous research on phonon dispersions on this system. The anomalies of $\rho(T)$ and $\chi(T)$ disappear with increasing T_c when Sb is gradually substituted by Bi, as reported experimentally. [7] Though there is no direct evidence by diffraction experiments, it seems, then, the present consensus on this compound that there is no instability toward CDW, which would be contradicting to our result here. The spin polarization, not taken into account here, may be one of the possibilities to modify the nesting, for instance via the spin-orbit coupling, accounting for this discrepancy, but it is reported, at least for DOS, the effect matters little. [21] A similar discrepancy between negative phonon predictions [38, 44] and unobserved structural instability is known for a superconductor, $\text{LaO}_{0.5}\text{F}_{0.5}\text{BiS}_2$. [45] A large phonon instability toward a static CDW was estimated theoretically, [38] while no anomaly in $\rho(T)$ and $\chi(T)$ has been observed experimentally. [45, 47] Yildirim [38] then argued the possibility of an unconventional superconducting mechanism in which inherent lattice instabilities have an important role on the Cooper pairing in this compound. A more recent neutron diffraction experiment [48] reported that the local distortion of the atomic position of S around Bi is detected under T_c , attracting an attention in connection with the unconventional mechanism. In our case of $\text{BaTi}_2\text{Bi}_2\text{O}$, the stabilization energy is evaluated around 23.3 meV/UnitCell, being much larger than that of $\text{LaO}_{0.5}\text{F}_{0.5}\text{BiS}_2$ (~ 10 meV/UnitCell). [38] In terms of the magnitude of the displacement, it is 0.16 Å for $\text{BaTi}_2\text{Bi}_2\text{O}$ (See Supplementary Note 4), which is the same as 0.16 Å for $\text{LaO}_{0.5}\text{F}_{0.5}\text{BiS}_2$. [38] In addition, the $\sqrt{2} \times \sqrt{2} \times 1$ superlattice structure obtained by analyzing dynamical matrices for $\text{BaTi}_2\text{Bi}_2\text{O}$ does not show any negative phonon frequency (Fig. 7 (c)). Therefore, the lattice instability is also expected to be static. The similarity might imply the similar unconventional mechanism also for $\text{BaTi}_2\text{Bi}_2\text{O}$. If it were so, the substitution of Sb by Bi would introduce the unconventionality to the conventional BCS of

$\text{BaTi}_2\text{Sb}_2\text{O}$. [16–18] The introduction might account for the two-dome structure appeared by the substitution. [8]

Possible mechanism for variety of superlattices

A natural question consequently arising would be asking why the new nesting vectors $\vec{k}_{||}^{(2)}$ appear only for $Pn = \text{As}$. The vectors are caused by the flattening of the 'nose' of Fermi surfaces directing toward the central cylinder from four equivalent outsides. Interestingly, the similar flattened 'nose' was actually reported in the paper by Singh *et al.* [21] (in their Fig. 7), shown as the 'Fermi surfaces' below E_F by 0.1 eV for $Pn = \text{Sb}$. Looking at our Fig. 2, we observe that the Fermi level seems to be approaching down toward the DOS peak as Pn changes from Bi and Sb to As. This can be regarded as if E_F effectively behaves like the 'sea-level down' $Pn = \text{As}$ with a fixed landscape of $Pn = \text{Sb}$. The Fermi surface of $Pn = \text{As}$ would therefore correspond to that of $Pn = \text{Sb}$ with negative energy shift, as shown in 'Fig. 7 by Singh *et al.*'. [21] The 'fixed landscape', namely the 'rigid band picture' near to Fermi level, can be justified to some extent because they are mainly composed of Ti- d orbital contributions as shown in Fig. 2. The reason why the 'sea-level' gets down when Pn is substituted into As can roughly be accounted as follows: As a rough estimation of how Pn affects to shift E_F , we can start with its 'HOMO' level of the isolated atom [HOMO stands for 'Highest Occupied Molecular Orbital' though the orbitals in the present context is not molecular but isolated atomic orbital. We use 'HOMO' rather than HOAO just because the latter is not so commonly spread abbreviation. We expect this doesn't matter so much even it is used for isolated atom.]. Namely, a negatively deeper 'HOMO' would contribute to attract Ti-electrons more strongly and make E_F lower. Noticing the deeper 'HOMO' corresponds to the larger ionic potential, we expect that the lighter element (As) has deeper 'HOMO' because the potential is enhanced by the less screening of the nucleus attractions by fewer inner electrons. [58] The deeper 'HOMO' also corresponds to the larger electronegativity, which is actually 2.18 for As while 2.05 (2.02) for Sb (Bi) by Pauling scale. Similar negativities for Sb and Bi can account for the common nesting vectors of these compounds, being different from that of As. Summarizing the above, the negatively deeper 'HOMO' level of As can attract Ti-electrons more strongly and effectively push E_F down when it forms pnictides, and then the Fermi surface changes to get flattened 'nose' as depicted in 'Fig. 7 of Singh *et al.* [21]'.

Though we could not make clear explanations here, we must note that the nesting vector cannot solely account for the superlattice instabilities even in the present case. In addition to $\vec{k}_{||}^{(2)}$ for $Pn = \text{As}$, $\vec{k}_{||}^{(1)}$ and $\vec{k}_{||}$ may be regarded as possible nesting vectors. The Kohn anomalies corresponding to $\vec{k}_{||}^{(1)}$ and $\vec{k}_{||}$ are, however, not present in the phonon dispersion. This fact might be related to recent intensive discussions about the Kohn anomaly [59]: Some studies [39–43] insist that the

imaginary phonons in quasi 2D systems are dominated not mainly by the nesting of electronic structures but rather primarily by the wave vector dependence of the electron-phonon coupling, $g(\vec{q})$. There exists, however, such quasi 2D systems [60] where their superlattice instabilities can clearly be explained by the nesting vectors. To investigate if our system corresponds to which case or that lying in between, it is quite intriguing to analyze $g(\vec{q})$ for $Pn = \text{As}$, but unfortunately we cannot perform any of such phonon calculations under the perfect disappearance of imaginary frequencies because of too costly calculations for the $2 \times 2 \times 1$ superlattice.

METHODS

All the calculations were done within DFT using GGA-PBE exchange-correlation functionals [49], implemented in Quantum Espresso package. [50] After carefully examining the artifacts due to the choice of pseudo potentials (PP), we provide here the final results mainly obtained by the PAW [51] framework of the valence/core separation of electrons. The implementation of PAW adopted here takes into account the relativistic effects within the extent of the scalar-relativistic theory upon a careful comparison with all-electron calculations by Wien2k. [52] We restricted ourselves to spin unpolarized calculations, anticipating that the spin polarization affects little as supported by several experiments. [16–18] Lattice instabilities are detected by the negative (imaginary) phonon dispersions evaluated for undistorted lattice structures. Taking each of the negative phonon modes, the structural relaxations along the mode are evaluated by the BFGS optimization scheme with the structural symmetries fixed to $Pbmm$ ($1 \times 2 \times 1$) and $Pbam$ ($2 \times 2 \times 1$) for $\text{BaTi}_2\text{As}_2\text{O}$, $P4/mbm$ ($\sqrt{2} \times \sqrt{2} \times 1$) for $\text{BaTi}_2\text{Sb}_2\text{O}$ and $\text{BaTi}_2\text{Bi}_2\text{O}$. For phonon calculations, we used the linear response theory implemented in Quantum Espresso package. [53] Crystal structures and Fermi surfaces are depicted by using VESTA [54] and XCrySDen [55], respectively.

To deal with the three compounds systematically, we took the same conditions for plane-wave cutoff energies (E_{cut}), k -meshes, and smearing parameters. The most strict condition among the compounds is taken to achieve the convergence within ± 1.0 mRy in the ground state energies of undistorted (superlattice) systems, resulting in $E_{\text{cut}}^{\text{(WF)}} = 90$ (100) Ry for wavefunction and $E_{\text{cut}}^{(\rho)} = 800$ (800) Ry for charge densities. For T_c evaluation, we adopted unshifted k -meshes centered at Γ -point. Denser k -meshes should be taken for electron-phonon calculations because of the double-delta integrations. [56] For undistorted systems, ($8 \times 8 \times 4$) k -meshes were used for the Brillouin-zone integration. Phonon dispersions were calculated on ($8 \times 8 \times 4$) q -meshes. Denser k -meshes, ($24 \times 24 \times 12$), were used for the double-delta integrations in electron-phonon calculations. For distorted $\text{BaTi}_2\text{As}_2\text{O}$ superlattices, ($8 \times 4 \times 4$) and ($4 \times 4 \times 4$) k -meshes were used for $1 \times 2 \times 1$ and $2 \times 2 \times 1$ superlattices, respectively.

Phonon dispersions were calculated on ($8 \times 4 \times 4$) and ($4 \times 4 \times 4$) q -meshes. Denser k -meshes, ($24 \times 12 \times 12$), were used for the double-delta integrations in electron-phonon calculations of the $1 \times 2 \times 1$ superlattice. For distorted $\text{BaTi}_2\text{Sb}_2\text{O}$ and $\text{BaTi}_2\text{Bi}_2\text{O}$ superlattices, ($6 \times 6 \times 6$) k -meshes are used. Phonon dispersions were calculated on ($6 \times 6 \times 6$) q -meshes. Denser k -meshes, ($18 \times 18 \times 18$), were used for the double-delta integrations in electron-phonon calculations. The Marzari-Vanderbilt cold smearing scheme [57] with a broadening width of 0.01 Ry was applied to all the compounds. To estimate T_c , we used Allen-Dynes formula [13, 14] implemented in Quantum Espresso, [50] with the effective Coulomb interaction μ^* , being chosen 0.1 empirically (See Supplementary Note 3).

REFERENCES

- [1] III, E. A., Ozawa, T., Kauzlarich, S. M. & Singh, R. R. Phase Transition and Spin-gap Behavior in a Layered Tetragonal Pnictide Oxide. *Journal of Solid State Chemistry* **134**, 423–426 (1997).
- [2] Ozawa, T. C., Kauzlarich, S. M., Bieringer, M., & Greedan, J. E. Possible Charge-Density-Wave/Spin-Density-Wave in the Layered Pnictide-Oxides: $\text{Na}_2\text{Ti}_2\text{Pn}_2\text{O}$ ($Pn = \text{As}, \text{Sb}$). *Chemistry of Materials* **13**, 1804–1810 (2001).
- [3] Liu, R. H. *et al.* Physical properties of the layered pnictide oxides $\text{Na}_2\text{Ti}_2\text{P}_2\text{O}$ ($P = \text{As}, \text{Sb}$). *Phys. Rev. B* **80**, 144516 (2009).
- [4] Wang, X. F. *et al.* Structure and physical properties for a new layered pnictide-oxide: $\text{BaTi}_2\text{As}_2\text{O}$. *Journal of Physics: Condensed Matter* **22**, 075702 (2010).
- [5] Yajima, T. *et al.* Superconductivity in $\text{BaTi}_2\text{Sb}_2\text{O}$ with a d^1 square lattice. *Journal of the Physical Society of Japan* **81**, 103706 (2012).
- [6] Doan, P. *et al.* $\text{Ba}_{1-x}\text{Na}_x\text{Ti}_2\text{Sb}_2\text{O}$ ($0.0 \leq x \leq 0.33$) A Layered Titanium-Based Pnictide Oxide Superconductor. *Journal of the American Chemical Society* **134**, 16520–16523 (2012).
- [7] Yajima, T. *et al.* Synthesis and Physical Properties of the New Oxybismuthides $\text{BaTi}_2\text{Bi}_2\text{O}$ and $(\text{SrF})_2\text{Ti}_2\text{Bi}_2\text{O}$ with a d^1 Square Net. *Journal of the Physical Society of Japan* **82**, 013703 (2013).
- [8] Yajima, T. *et al.* Two Superconducting Phases in the Isovalent Solid Solutions $\text{BaTi}_2\text{Pn}_2\text{O}$ ($Pn = \text{As}, \text{Sb}, \text{and Bi}$). *Journal of the Physical Society of Japan* **82**, 033705 (2013).
- [9] Zhai, H.-F. *et al.* Superconductivity, charge- or spin-density wave, and metal-nonmetal transition in $\text{BaTi}_2(\text{Sb}_{1-x}\text{Bi}_x)_2\text{O}$. *Phys. Rev. B* **87**, 100502 (2013).
- [10] Nakano, K. *et al.* T_c Enhancement by Aliovalent Anionic Substitution in Superconducting $\text{BaTi}_2(\text{Sb}_{1-x}\text{Sn}_x)_2\text{O}$. *Journal of the Physical Society of Japan* **82**, 074707 (2013).
- [11] Pachmayr, U. & Johrendt, D. Superconductivity in $\text{Ba}_{1-x}\text{K}_x\text{Ti}_2\text{Sb}_2\text{O}$ ($0 \leq x \leq 1$) controlled by the layer charge. *Solid State Sciences* **28**, 31–34 (2014).
- [12] von Rohr, F., Nesper, R. & Schilling, A. Superconductivity in rubidium-substituted $\text{Ba}_{1-x}\text{Rb}_x\text{Ti}_2\text{Sb}_2\text{O}$. *Phys. Rev. B* **89**, 094505 (2014).
- [13] Bardeen, J., Cooper, L. N. & Schrieffer, J. R. Theory of superconductivity. *Phys. Rev.* **108**, 1175 (1957).

- [14] Allen, P. B. & Dynes, R. C. Transition temperature of strongly coupled superconductors reanalyzed. *Phys. Rev. B* **12**, 905–922 (1965).
- [15] Subedi, A. Electron-phonon superconductivity and charge density wave instability in the layered titanium-based pnictide $\text{BaTi}_2\text{Sb}_2\text{O}$. *Phys. Rev. B* **87**, 054506 (2013).
- [16] Kitagawa, S., Ishida, K., Nakano, K., Yajima, T. & Kageyama, H. *s*-wave superconductivity in superconducting $\text{BaTi}_2\text{Sb}_2\text{O}$ revealed by $^{121/123}\text{Sb}$ -NMR/nuclear quadrupole resonance measurements. *Phys. Rev. B* **87**, 060510 (2013).
- [17] Nozaki, Y. *et al.* Muon spin relaxation and electron/neutron diffraction studies of $\text{BaTi}_2(\text{As}_{1-x}\text{Sb}_x)_2\text{O}$: Absence of static magnetism and superlattice reflections. *Phys. Rev. B* **88**, 214506 (2013).
- [18] von Rohr, F., Schilling, A., Nesper, R., Baines, C. & Bendele, M. Conventional superconductivity and charge-density-wave ordering in $\text{Ba}_{1-x}\text{Na}_x\text{Ti}_2\text{Sb}_2\text{O}$. *Phys. Rev. B* **88**, 140501 (2013).
- [19] Bednorz, J. & Müller, K. Possible high- T_c superconductivity in the Ba-La-Cu-O system. *Zeitschrift für Physik B Condensed Matter* **64**, 189–193 (1986).
- [20] Kamihara, Y., Watanabe, T., Hirano, M. & Hosono, H. Iron-Based Layered Superconductor $\text{La}[\text{O}_{1-x}\text{F}_x]\text{FeAs}$ ($x = 0.05 - 0.12$) with $T_c = 26$ K. *Journal of the American Chemical Society* **130**, 3296–3297 (2008).
- [21] Singh, D. J. Electronic structure, disconnected Fermi surfaces and antiferromagnetism in the layered pnictide superconductor $\text{Na}_x\text{Ba}_{1-x}\text{Ti}_2\text{Sb}_2\text{O}$. *New Journal of Physics* **14**, 123003 (2012).
- [22] Wang, G., Zhang, H., Zhang, L. & Liu, C. The electronic structure and magnetism of $\text{BaTi}_2\text{Sb}_2\text{O}$. *Journal of Applied Physics* **113** (2013).
- [23] Yu, X.-L. *et al.* A site-selective antiferromagnetic ground state in layered pnictide-oxide $\text{BaTi}_2\text{As}_2\text{O}$. *Journal of Applied Physics* **115**, 17A924 (2014).
- [24] Suetin, D. & Ivanovskii, A. Electronic properties and Fermi surface for new Fe-free layered pnictide-oxide superconductor $\text{BaTi}_2\text{Bi}_2\text{O}$ from first principles. *JETP Letters* **97**, 220–225 (2013).
- [25] Xu, H. C. *et al.* Electronic structure of the $\text{BaTi}_2\text{As}_2\text{O}$ parent compound of the titanium-based oxypnictide superconductor. *Phys. Rev. B* **89**, 155108 (2014).
- [26] Song, Q. *et al.* Electronic structure of the titanium-based oxypnictide superconductor $\text{Ba}_{0.95}\text{Na}_{0.05}\text{Ti}_2\text{Sb}_2\text{O}$ and direct observation of its charge density wave order. *Phys. Rev. B* **93**, 024508 (2016).
- [27] Frandsen, B. A. *et al.* Intra-unit-cell nematic charge order in the titanium-oxypnictide family of superconductors. *Nat. Commun.* **5**, 5761 (2014).
- [28] Lawler, M. J. *et al.* Intra-unit-cell electronic nematicity of the high- T_c copper-oxide pseudogap states. *Nature* **466**, 347–351 (2010).
- [29] Fujita, K. *et al.* Direct phase-sensitive identification of a *d*-form factor density wave in underdoped cuprates. *Proceedings of the National Academy of Sciences* **111**, E3026 (2014).
- [30] Koike, Y., Watanabe, N., Noji, T. & Saito, Y. Effects of the Cu-site substitution on the anomalous x dependence of T_c in $\text{La}_{2-x}\text{Ba}_x\text{CuO}_4$. *Solid State Communications* **78**, 511–514 (1991).
- [31] Koike, Y., Kawaguchi, T., Watanabe, N., Noji, T. & Saito, Y. Superconductivity and low-temperature structural phase transition in $\text{La}_{1.98-x}\text{Ce}_{0.02}\text{Ba}_x\text{CuO}_4$. *Solid State Communications* **79**, 155–158 (1991).
- [32] Tamegai, T. & Iye, Y. Universal transport anomaly in $\text{YBa}_2\text{Cu}_3\text{O}_{7-y}$ -type systems with reduced carrier density. *Phys. Rev. B* **44**, 10167 (1991).
- [33] Koike, Y. *et al.* Anomalous x dependence of T_c and possibility of low-temperature structural phase transition in $\text{La}_{2-x}\text{Sr}_x\text{Cu}_{0.99}\text{M}_{0.01}\text{O}_4$ ($M = \text{Ni}, \text{Zn}, \text{Ga}$). *Solid State Communications* **82**, 889–893 (1992).
- [34] Ando, Y., Komiya, S., Segawa, K., Ono, S. & Kurita, Y. Electronic Phase Diagram of High- T_c Cuprate Superconductors from a Mapping of the In-Plane Resistivity Curvature. *Phys. Rev. Lett.* **93**, 267001 (2004).
- [35] Iimura, S. *et al.* Two-dome structure in electron-doped iron arsenide superconductors. *Nat. Commun.* **3**, 943 (2012).
- [36] Matsuiishi, S., Maruyama, T., Iimura, S. & Hosono, H. Controlling factors of T_c dome structure in 1111-type iron arsenide superconductors. *Phys. Rev. B* **89**, 094510 (2014).
- [37] Fujiwara, N. *et al.* Detection of Antiferromagnetic Ordering in Heavily Doped $\text{LaFeAsO}_{1-x}\text{H}_x$ Pnictide Superconductors Using Nuclear-Magnetic-Resonance Techniques. *Phys. Rev. Lett.* **111**, 097002 (2013).
- [38] Yildirim, T. Ferroelectric soft phonons, charge density wave instability, and strong electron-phonon coupling in BiS_2 layered superconductors: A first-principles study. *Phys. Rev. B* **87**, 020506 (2013).
- [39] Johannes, M. D., Mazin, I. I. & Howells, C. A. Fermi-surface nesting and the origin of the charge-density wave in NbSe_2 . *Phys. Rev. B* **73**, 205102 (2006).
- [40] Johannes, M. D. & Mazin, I. I. Fermi surface nesting and the origin of charge density waves in metals. *Phys. Rev. B* **77**, 165135 (2008).
- [41] Calandra, M., Mazin, I. I. & Mauri, F. Effect of dimensionality on the charge-density wave in few-layer 2H-NbSe₂. *Phys. Rev. B* **80**, 241108 (2009).
- [42] Calandra, M. & Mauri, F. Charge-Density Wave and Superconducting Dome in TiSe_2 from Electron-Phonon Interaction. *Phys. Rev. Lett.* **106**, 196406 (2011).
- [43] Zhu, X., Cao, Y., Zhang, J., Plummer, E. W., & Guo, J. Classification of charge density waves based on their nature. *Proc. Natl. Acad. Sci. USA* **112**, 2367–2371 (2015).
- [44] Wan, X., Ding, H.-C., Savrasov, S. Y. & Duan, C.-G. Electron-phonon superconductivity near charge-density-wave instability in $\text{LaO}_{0.5}\text{F}_{0.5}\text{BiS}_2$: Density-functional calculations. *Phys. Rev. B* **87**, 115124 (2013).
- [45] Mizuguchi, Y. *et al.* Superconductivity in novel BiS_2 -based layered superconductor $\text{LaO}_{1-x}\text{F}_x\text{BiS}_2$. *Journal of the Physical Society of Japan* **81**, 114725 (2012).
- [46] Aroyo, M. I. *et al.* Brillouin-zone databases on the Bilbao Crystallographic Server. *Acta Cryst.* **A70**, 126–137 (2014).
- [47] Lee, J. *et al.* Crystal structure, lattice vibrations, and superconductivity of $\text{LaO}_{1-x}\text{F}_x\text{BiS}_2$. *Phys. Rev. B* **87**, 205134 (2013).
- [48] Athauda, A. *et al.* In-plane charge fluctuations in bismuth-sulfide superconductors. *Phys. Rev. B* **91**, 144112 (2015).
- [49] Perdew, J. P., Burke, K. & Ernzerhof, M. Generalized Gradient Approximation Made Simple. *Phys. Rev. Lett.* **77**, 3865 (1996).
- [50] Giannozzi, P. *et al.* QUANTUM ESPRESSO: a modular and open-source software project for quantum simulations of materials. *Journal of Physics: Condensed Matter* **21**, 395502 (2009).
- [51] Blöchl, P. E. Projector augmented-wave method. *Phys. Rev. B* **50**, 17953 (1994).
- [52] Jollet, F., Torrent, M. & Holzwarth, N. Generation of projector augmented-wave atomic data: A 71 element validated table in the XML format. *Computer Physics Communications* **185**, 1246–1254 (2014).
- [53] Baroni, S., de Gironcoli, S., Dal Corso, A. & Giannozzi, P. Phonons and related crystal properties from density-functional perturbation theory. *Rev. Mod. Phys.* **73**, 515 (2001).

- [54] Momma, K. & Izumi, F. VESTA3 for three-dimensional visualization of crystal, volumetric and morphology data. *Journal of Applied Crystallography* **44**, 1272–1276 (2011).
- [55] Kokalj, A. XCrySDen—a new program for displaying crystalline structures and electron densities. *Journal of Molecular Graphics and Modelling* **17**, 176–179 (1999).
- [56] Wierzbowska, M., de Gironcoli, S. & Giannozzi, P. Origins of low- and high-pressure discontinuities of T_c in niobium. *eprint arXiv:cond-mat/0504077* (2006).
- [57] Marzari, N., Vanderbilt, D., De Vita, A. & Payne, M. C. Thermal Contraction and Disordering of the Al(110) Surface. *Phys. Rev. Lett.* **82**, 3296 (1999).
- [58] Hongo, K., Interpretation of Hund’s multiplicity rule for the carbon atom. *J. Chem. Phys.* **121**, 7144–7147 (2004).
- [59] Kohn, W., Image of the Fermi Surface in the Vibration Spectrum of a Metal. *Phys. Rev. Lett.* **2**, 393–394 (1959).
- [60] Kim, H., Kang, C., Kim, K., Shim, J. H., & Min, B. I. Phonon softenings and the charge density wave instability in R_2O_2Sb (R = rare-earth element). *Phys. Rev. B* **91**, 165130 (2015).

ACKNOWLEDGMENTS

The authors are grateful to Tomohiro Ichibha for assistance in DFT calculation, Takeshi Yajima for useful discussion, and Hiroshi Kageyama for his encouragement. The authors also acknowledge the support by the Computational Materials Science Initiative (CMSI/Japan) for the computational resources, Project Nos. hp120086, hp140150, hp150014 at K-computer, and SR16000 (Center for Computational Materials Science of the Institute for Materials Research, Tohoku University/Japan). R.M. is grateful for financial support from MEXT-KAKENHI grants 26287063, 25600156, 22104011 and that from the Asahi glass Foundation. K.H. is grateful for financial support from MEXT-KAKENHI grants 15K21023 and 15H02672. The computation in this work has been partially performed using the facilities of the Center for Information Science in JAIST.

AUTHOR CONTRIBUTIONS

K.N. initiated and performed main calculations under the supervision by R.M. Data is analysed by K.N. and K.H. All the authors wrote the paper, section by section, finally organized to a manuscript.

ADDITIONAL INFORMATION

Competing financial interests: The authors declare no competing financial interests.

SUPPLEMENTARY INFORMATION

Supplementary Note 1

Our optimized geometry parameters for undistorted structures are given in Table S-I, compared with experimental values. The optimizations were performed under a fixed symmetry, $P4/mmm$, to relax both lattice parameters, a and c , and internal coordinations within a primitive cell. For a and the internal coordinations, our results are in good agreements with experiments, while those for c are slightly longer than the experimental values. This trend is also reported in previous calculations by Suetin *et al.* [S1, S2]. This is due to our choice of GGA-PBE, which is known to overestimate lattice parameters in general [S3].

TABLE S-I. Optimized lattice constants, a ($= b$) and c , and z -components of Pn atomic positions of $BaTi_2Pn_2O$ ($Pn = As, Sb, Bi$) under $P4/mmm$ symmetry, compared with experiments and other DFT results. All units are given in Å.

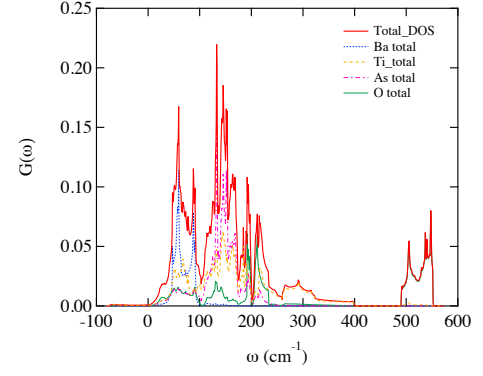
$BaTi_2As_2O$	a	c	As z-pos.
GGA-PBE (previous) [S2]	4.057	7.263	0.2427
GGA-PBE (present)	4.058	7.393	0.2422
Experiment [S4]	4.046	7.272	0.2440
$BaTi_2Sb_2O$	a	c	Sb z-pos.
GGA-PBE (previous) [S2]	4.116	8.107	0.2467
GGA-PBE (present)	4.089	8.285	0.2451
Experiment [S5]	4.110	8.086	0.2487
$BaTi_2Bi_2O$	a	c	Bi z-pos.
GGA-PBE (previous) [S1]	4.122	8.547	0.2523
GGA-PBE (present)	4.118	8.630	0.2481
Experiment [S6]	4.123	8.345	0.2513

Supplementary Note 2

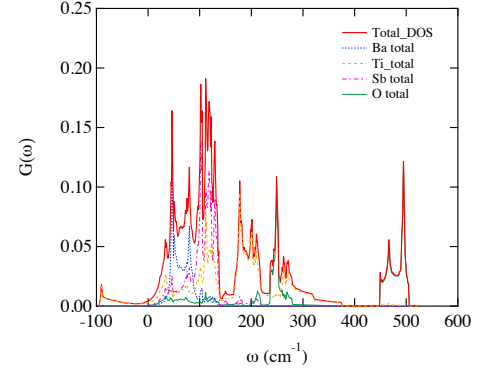
From phonon pDOS (partial DOS), we can identify which vibration modes lead to the instability toward the superlattice. We got pDOS with using QHA module which is implemented in Quantum espresso. [S7] For undistorted $Pn=Sb$ and Bi , it is found from Figs. S-1 and S-2 that the negative (imaginary) frequencies mainly come from Ti 'in-plane' (within xy plane) vibrations. This is consistent with the previous calculation by Subedi [S8] for $Pn=Sb$. It is found from Fig. S-3 that the negative frequencies of undistorted $Pn=As$ comes from Ti and As 'in-plane' vibrations. Finally, we concluded that only 'in-plane' vibrations contribute to the negative frequencies for all the compound.

Supplementary Note 3

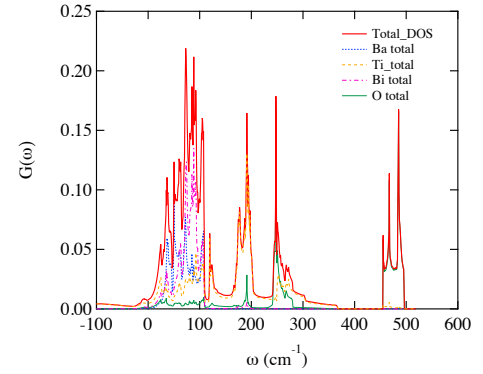
To estimate T_c , we used Allen-Dynes formula [S9, S10] implemented in Quantum Espresso, [S7]



(a) $BaTi_2As_2O$



(b) $BaTi_2Sb_2O$



(c) $BaTi_2Bi_2O$

FIG. S-1. Total and partial phonon density of states of $BaTi_2Pn_2O$ under $P4/mmm$ symmetry ($Pn =$ (a) As, (b) Sb, and (c) Bi).

$$T_c = \frac{\omega_{ln}}{1.2} \exp \left[\frac{-1.04(1 + \lambda)}{\lambda - \mu^*(1 + 0.62\lambda)} \right], \quad (1)$$

where

$$\lambda = 2 \int d\omega \frac{\alpha^2 F(\omega)}{\omega} \quad (2)$$

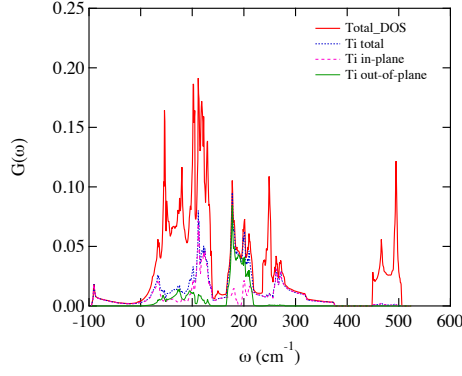
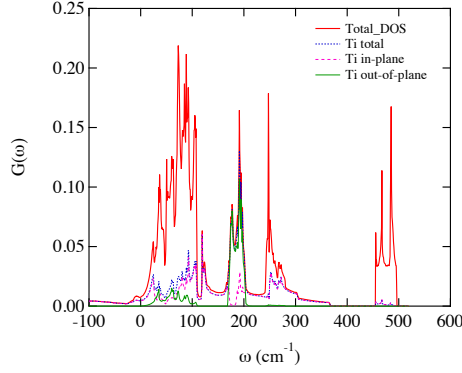
(a) $\text{BaTi}_2\text{Sb}_2\text{O}$ (b) $\text{BaTi}_2\text{Bi}_2\text{O}$

FIG. S-2. Partial density of states for phonons in $\text{BaTi}_2Pn_2\text{O}$ ($Pn = \text{Sb}$ and Bi), divided into the contributions from in-plane and out-of-plane vibrations of Ti atoms.

denotes the frequency-averaged electron-phonon coupling constant, and

$$\omega_{\text{ln}} = \exp \left[\frac{2}{\lambda} \int d\omega \alpha^2 F(\omega) \frac{\ln \omega}{\omega} \right] \quad (3)$$

denotes logarithm-averaged phonon frequency. The constant, μ^* , describes the effective Coulomb interaction, being chosen 0.1 empirically. Eliashberg function [S11] is given as

$$\alpha^2 F(\omega) = \frac{1}{2\pi N(\varepsilon_F)} \sum_{q,v} \delta(\omega - \omega_{q,v}) \frac{\gamma_{q,v}}{\hbar \omega_{q,v}}, \quad (4)$$

where $N(\varepsilon_F)$, $\omega_{q,v}$, and $\gamma_{q,v}$ denote the density of state at Fermi-level, phonon frequency, and relaxation constant for a mode (q, v) , respectively.

Following the above equation, T_c are estimated for undistorted and superlattice structures $Pn = \text{As}$, Sb and Bi cases. Eliashberg functions are shown in Fig. S-4 (undistorted structures) and in Fig. S-5 (superlattice structures). The parameters appearing in the formula are also tabulated in the table S-II. Our estimated values, $T_c = 2.30$ (2.45) K for superlattice structures of $Pn = \text{Sb}$ (Bi) which show no imaginary frequency, are consistent with experimental values $T_c = 1.2$

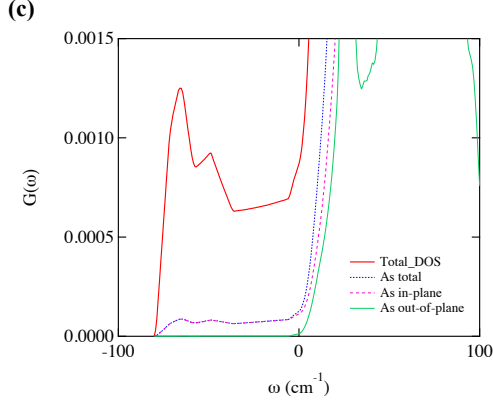
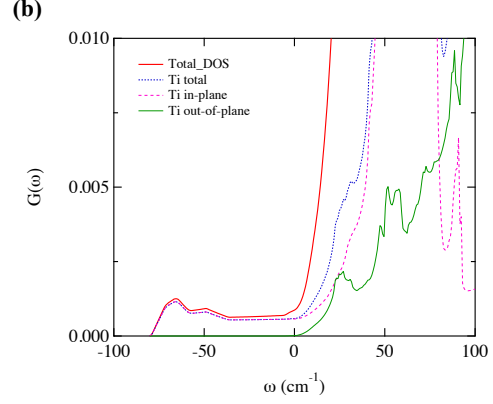
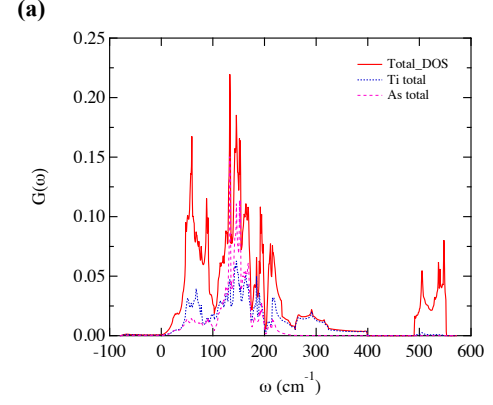


FIG. S-3. Partial density of states for phonons in $\text{BaTi}_2\text{As}_2\text{O}$, divided into the contributions from in-plane and out-of-plane vibrations of Ti and As atoms.

(4.6) K for $Pn = \text{Sb}$ (Bi). This evaluation, however, assumes a simple BCS-type mechanism, which might be debatable for $\text{BaTi}_2\text{Bi}_2\text{O}$ as mentioned in the main article. As for $Pn = \text{As}$, T_c were estimated only for the unstable structures which show imaginary frequencies. Therefore, the estimated value $T_c = 6.93$ K ($1 \times 1 \times 1$), 8.31 K ($1 \times 2 \times 1$) are not compatible with the experimental fact that $\text{BaTi}_2\text{As}_2\text{O}$ does not show any superconductivity. [S4, S13]

TABLE S-II. T_c obtained by Allen-Dynes formula for $\text{BaTi}_2Pn_2\text{O}$ ($Pn = \text{As}, \text{Sb}, \text{and Bi}$)

Compounds (structures)	Present calculations			Previous calculations			Experiments
	λ	ω_{ln}	T_c	λ	ω_{ln}	T_c	T_c
$\text{BaTi}_2\text{As}_2\text{O}$ ($1 \times 1 \times 1$)	1.37	66.56 K	6.93 K	-	-	-	- [S4, S13]
$\text{BaTi}_2\text{Sb}_2\text{O}$ ($1 \times 1 \times 1$)	0.62	90.44 K	2.23 K	1.28 [S8]	93.52 K [S8]	9.0 K [S8]	1.2 K [S5]
$\text{BaTi}_2\text{Bi}_2\text{O}$ ($1 \times 1 \times 1$)	0.84	74.99 K	3.89 K	-	-	-	4.6 K [S6]
$\text{BaTi}_2\text{As}_2\text{O}$ ($1 \times 2 \times 1$)	0.92	137.10 K	8.31 K	-	-	-	- [S4, S13]
$\text{BaTi}_2\text{Sb}_2\text{O}$ ($\sqrt{2} \times \sqrt{2} \times 1$)	0.52	165.91 K	2.30 K	0.55 [S8]	110 K [S8]	2.7 K [S8]	1.2 K [S5]
$\text{BaTi}_2\text{Bi}_2\text{O}$ ($\sqrt{2} \times \sqrt{2} \times 1$)	0.56	134.39 K	2.45 K	-	-	-	4.6 K [S6]

Supplementary Note 4

In general, we can predict superlattice structures by analyzing dynamical matrices. Once we identify the symmetries, we can perform geometry optimizations for the superlattice under the identified symmetries and get relaxed geometry of the superlattice structures. We found that the lattice instabilities in $Pn = \text{Sb}$ and Bi induce structural transition from $P4/mmm$ (No.123) to $P4/mbm$ (No.127) by analyzing dynamical matrices. The results of geometry optimization under the identified symmetry ($P4/mbm$) are shown in Tables S-IV and S-V. On the other hand, we found that the lattice instabilities in $Pn = \text{As}$ induce structural transition from $P4/mmm$ (No.123) to $Pbmm$ (No.51), which is different from $Pn = \text{Sb}$ and Bi . The results of geometry optimization under the identified symmetry ($Pbmm$) are summarized in Table S-III. As mentioned in the main article, the superlattice structure of $Pn = \text{As}$ ($1 \times 2 \times 1$) still shows imaginary frequencies. We, therefore, further analyzed dynamical matrices and found the structural transition from $Pbmm$ (No.51) to $Pbam$ (No.55). The results of geometry optimization under the identified symmetry ($Pbam$) are summarized in Table S-VI. The results in Tables S-III-S-VI are compared with experiments and discussed in the main article.

TABLE S-III. Internal atomic positions of $\text{BaTi}_2\text{As}_2\text{O}$ superlattice structure ($1 \times 2 \times 1$, No.51 $Pbmm$), given in fractional coordinates for the lattice constants, $a = 4.060 \text{ \AA}$, $b = 8.110 \text{ \AA}$, and $c = 7.401 \text{ \AA}$. All the atomic positions and lattice constants are simultaneously optimized by GGA-PBE. The magnitude of distortions in terms of the orthogonal index is evaluated as, $\eta = 2 \times (a - 1/2b)/(a + 1/2b) = 0.115\%$, being fairly coincidence with the experimental value from neutron diffraction, [S12] $\eta = 0.22\%$.

Atom Site	x	y	z
Ba	$2d$	0.5000	0.5000
Ti	$2a$	0.0000	0.0000
Ti	$2e$	0.4851	0.2500
As	$4k$	0.0040	0.2500
O	$2c$	0.5000	0.0000

TABLE S-IV. Internal atomic positions of $\text{BaTi}_2\text{Sb}_2\text{O}$ superlattice structure ($\sqrt{2} \times \sqrt{2} \times 1$, No.127 $P4/mbm$), given in fractional coordinates for the lattice constants, $a = b = 5.791 \text{ \AA}$ and $c = 8.349 \text{ \AA}$. All the atomic positions and lattice constants are simultaneously optimized by GGA-PBE. Ti atom displaces by 0.14 \AA from its original high-symmetric position.

Atom Site	x	y	z
Ba	$2b$	0.5000	0.5000
Ti	$4g$	0.7326	0.2674
Sb	$4f$	0.0000	0.5000
O	$2a$	0.0000	0.0000

TABLE S-V. Internal atomic positions of $\text{BaTi}_2\text{Bi}_2\text{O}$ superlattice structure ($\sqrt{2} \times \sqrt{2} \times 1$, No.127 $P4/mbm$), given in fractional coordinates for the lattice constants, $a = b = 5.808 \text{ \AA}$ and $c = 8.687 \text{ \AA}$. All the atomic positions and lattice constants are simultaneously optimized by GGA-PBE. Ti atom displaces by 0.16 \AA from its original high-symmetric position.

Atom Site	x	y	z
Ba	$2b$	0.5000	0.5000
Ti	$4g$	0.7309	0.2691
Bi	$4f$	0.0000	0.5000
O	$2a$	0.0000	0.0000

TABLE S-VI. Internal atomic positions of $\text{BaTi}_2\text{As}_2\text{O}$ superlattice structure ($2 \times 2 \times 1$, No.55 $Pbam$), given in fractional coordinates for the lattice constants, $a = 8.122 \text{ \AA}$, $b = 8.108 \text{ \AA}$, and $c = 7.401 \text{ \AA}$. All the atomic positions and lattice constants are simultaneously optimized by GGA-PBE. The magnitude of distortions in terms of the orthorhombicity is evaluated as, $\eta = 2 \times (a - b)/(a + b) = 0.171\%$, being coincidence with the experimental value from neutron diffraction, [S12] $\eta = 0.22\%$.

Atom Site	x	y	z
Ba	$2a$	0.5000	0.5000
Ba	$2b$	0.0000	0.5000
Ti	$4g$	0.2500	0.5034
Ti	$4g$	0.0080	0.2500
As	$8i$	0.2519	0.2509
O	$2a$	0.0000	0.5000
O	$2c$	0.5000	0.0000

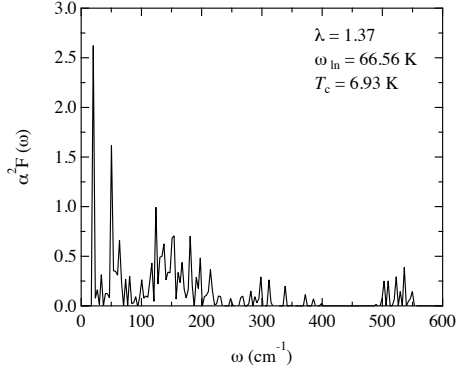
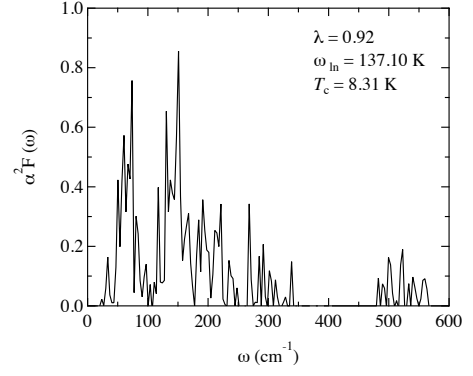
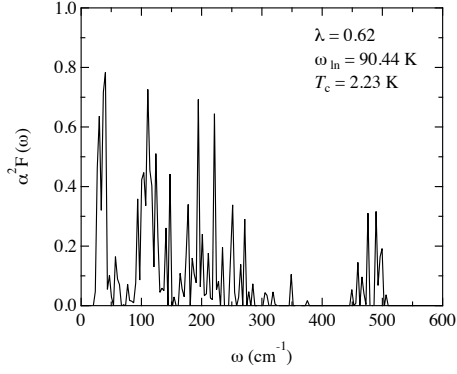
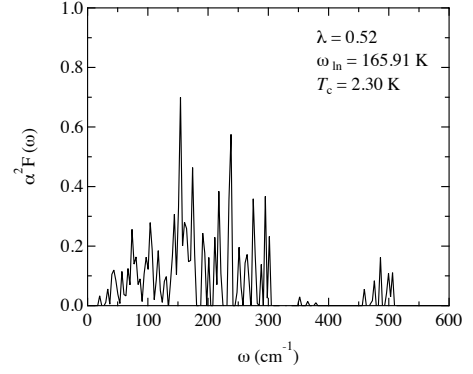
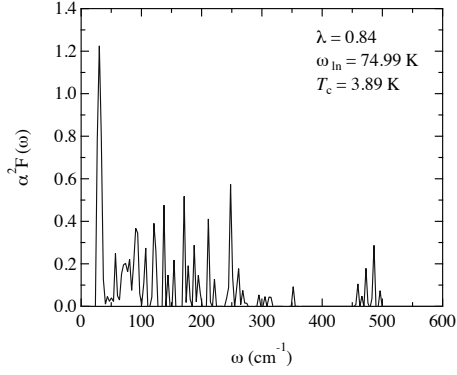
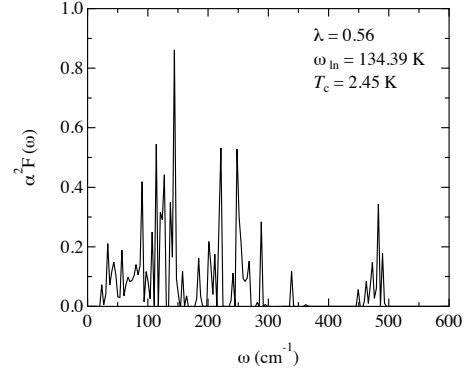
(a) $\text{BaTi}_2\text{As}_2\text{O}$ (a) $\text{BaTi}_2\text{As}_2\text{O}$ (b) $\text{BaTi}_2\text{Sb}_2\text{O}$ (b) $\text{BaTi}_2\text{Sb}_2\text{O}$ (c) $\text{BaTi}_2\text{Bi}_2\text{O}$ (c) $\text{BaTi}_2\text{Bi}_2\text{O}$

FIG. S-4. Eliashberg spectral function $\alpha^2 F(\omega)$ for (a) $\text{BaTi}_2\text{As}_2\text{O}$, (b) $\text{BaTi}_2\text{Sb}_2\text{O}$ and (c) $\text{BaTi}_2\text{Bi}_2\text{O}$ under $P4/mmm$ symmetry. The imaginary frequencies are not taken into account.

FIG. S-5. Eliashberg spectral function $\alpha^2 F(\omega)$ for superlattice structures, (a) $\text{BaTi}_2\text{As}_2\text{O}-1 \times 2 \times 1$, (b) $\text{BaTi}_2\text{Sb}_2\text{O}-\sqrt{2} \times \sqrt{2} \times 1$ and (c) $\text{BaTi}_2\text{Bi}_2\text{O}-\sqrt{2} \times \sqrt{2} \times 1$. The imaginary frequencies are not taken into account for $\text{BaTi}_2\text{As}_2\text{O}$.

[S1] Suetin, D. & Ivanovskii, A. Electronic properties and fermi surface for new Fe-free layered pnictide-oxide superconductor $\text{BaTi}_2\text{Bi}_2\text{O}$ from first principles. *JETP Letters* **97**, 220–225 (2013).

[S2] Suetin, D. & Ivanovskii, A. Structural, electronic properties, and chemical bonding in quaternary layered titanium

pnictide-oxides $\text{Na}_2\text{Ti}_2\text{Pn}_2\text{O}$ and $\text{BaTi}_2\text{Pn}_2\text{O}$ ($pn = \text{As}, \text{Sb}$) from FLAPW–GGA calculations. *Journal of Alloys and Compounds* **564**, 117–124 (2013).

[S3] Ouma, C. N. M., Mapelu, M. Z., Makau, N. W., Amolo, G. O. & Maezono, R. Quantum monte carlo study of pressure-induced $b3 - b1$ phase transition in GaAs. *Phys. Rev. B* **86**, 104115 (2012).

- [S4] Wang, X. F. *et al.* Structure and physical properties for a new layered pnictide-oxide: $\text{BaTi}_2\text{As}_2\text{O}$. *Journal of Physics: Condensed Matter* **22**, 075702 (2010).
- [S5] Yajima, T. *et al.* Superconductivity in $\text{BaTi}_2\text{Sb}_2\text{O}$ with a d^1 square lattice. *Journal of the Physical Society of Japan* **81**, 103706 (2012).
- [S6] Yajima, T. *et al.* Synthesis and Physical Properties of the New Oxybismuthides $\text{BaTi}_2\text{Bi}_2\text{O}$ and $(\text{SrF})_2\text{Ti}_2\text{Bi}_2\text{O}$ with a d^1 Square Net. *Journal of the Physical Society of Japan* **82**, 013703 (2013).
- [S7] Giannozzi, P. *et al.* QUANTUM ESPRESSO: a modular and open-source software project for quantum simulations of materials. *Journal of Physics: Condensed Matter* **21**, 395502 (2009).
- [S8] Subedi, A. Electron-phonon superconductivity and charge density wave instability in the layered titanium-based pnictide $\text{BaTi}_2\text{Sb}_2\text{O}$. *Phys. Rev. B* **87**, 054506 (2013).
- [S9] Bardeen, J., Cooper, L. N. & Schrieffer, J. R. Theory of superconductivity. *Phys. Rev.* **108**, 1175 (1957).
- [S10] Allen, P. B. & Dynes, R. C. Transition temperature of strong-coupled superconductors reanalyzed. *Phys. Rev. B* **12**, 905–922 (1965).
- [S11] Eliashberg, G. M. Interactions between electrons and lattice vibrations in a superconductor. *Sov. Phys.-JETP* **11**, 696–702 (1960).
- [S12] Frandsen, B. A. *et al.* Intra-unit-cell nematic charge order in the titanium-oxypnictide family of superconductors. *Nat. Commun.* **5**, 5761 (2014).
- [S13] Yajima, T. *et al.* Two Superconducting Phases in the Isovalent Solid Solutions $\text{BaTi}_2\text{Pn}_2\text{O}$ ($\text{Pn} = \text{As}, \text{Sb}, \text{and Bi}$). *Journal of the Physical Society of Japan* **82**, 033705 (2013).